J. Fluid Mech. (1969), *vol.* 37, *part* 1, *pp.* 115–127
Printed in Great Britain

The dynamic balances of dissolved air and heat in natural cavity flows

By C. BRENNEN†
Ship Division, National Physical Laboratory

(Received 22 March 1968)

In steady, fully developed and unventilated cavity flows occurring in practice, air (originally dissolved in the water) and heat are diffused through the fluid towards the interface providing a continuous supply of air and vapour to the cavity. This must be balanced by the rate of entrainment of volume of air and vapour away from the cavity in the wake. These equilibria which determine respectively the partial pressure of air within the cavity and the temperature differences involved in the flow are studied in this paper. The particular case of the cavitating flow past a spherical headform has been investigated in detail. Measurements indicate a near-linear relation between the partial pressure of air in the cavity and the total air content of the water. From a second set of experiments, designed to estimate the volume rates of entrainment under various conditions by employing artificial ventilation, it appears that this is a function only of tunnel speed and cavity size within the range of the experiments. A simplified theoretical approach involving the turbulent boundary layer on the surface of the cavity is then used to estimate the rates of diffusion into the cavity. The resulting air balance yields a partial pressure of air/air content relation compatible with experiment. The water vapour or heat balance suggests that the temperature differences involved are likely to be virtually undetectable experimentally.

1. Introduction

Previous experiments such as those of Gadd & Grant (1965) have demonstrated that the measured pressure within fully developed cavities, p_c, exceeds the water vapour pressure, p_v, because of the unavoidable presence of air (or other gas) dissolved in the liquid. This diffuses through the fluid and sets up a partial pressure of air, p_{AD}, in the cavity so that $p_c = p_v + p_{AD}$. The mass rate of supply of air by this diffusion process must clearly be matched, under steady conditions, by the rate at which air is entrained away from the cavity in its wake. Similarly, heat is diffused to the cavity and provides a continuous supply of water vapour by evaporation at the interface. The bubbles entrained and convected away in the wake will, at least initially, contain air and vapour in the same proportions as the cavity contents. Thus the two balances, one of dissolved air and one of heat, are interconnected.

This paper is concerned with demonstrating how the conditions of pressure and temperature within the cavity are dependent upon the balance between the rates

† Present address: California Institute of Technology, Pasadena, California.

of diffusion and entrainment. Clearly each of these two phenomena must be studied separately and theoretical expressions or experimental data obtained for each before the equilibrium equations determining the cavity conditions can be set up. The predicted conditions could then be compared with those measured experimentally.

To this end a relatively simple kind of cavity flow, namely, that behind a spherical headform in a horizontal water tunnel was chosen for particular investigation. Initial experiments showed that the partial pressure of air in the cavity was roughly proportional to the total air content of the water (§ 3). By making use of an artificial supply of air to the cavity (ventilation), a second set of experiments determined the behaviour and obtained values of the rates of entrainment of air and water vapour (§ 5). No attempt has been made to treat this process theoretically since it is clearly a complex kind of two-phase flow. On the other hand, since it is very difficult to envisage an experiment which would provide any measurement of the rates of diffusion, this phenomena was investigated theoretically (§ 6). The resulting air balance predicts partial pressures of air comparable with experiment and the heat balance suggests that the temperature differences are likely to be virtually undetectable experimentally.

2. Experimental arrangement

The experiments were carried out in the no. 2 water tunnel of Ship Division, N.P.L. (Silverleaf 1960), the spherical headform (3 in. diameter) being supported on the sting and strut system shown in figure 1. The same apparatus had earlier been used to investigate the length and separation position for natural cavities (Brennen 1968). Measurements of cavity length, L (defined in figure 1), were repeated for ventilated cavities and these results, which confirmed that the length/cavitation number relationship was negligibly different from that for natural cavities, are made use of in § 5. The cavitation number, σ, is defined as $(p_u - p_c)/\frac{1}{2}\rho U^2$, p_u and U being the pressure and velocity of the undisturbed stream in the tunnel and ρ the water density. In the present experiments three tubes opened on the back face of the headform; two of these were connected via a flow meter to an air supply for the purpose of ventilation; a mercury vacuum manometer connected to the third was used to measure cavity pressure, the actual technique employed being outlined in the next section.

The total air content of the water, P, measured in parts per million (p.p.m.) by weight using a Van Slyke apparatus, could be maintained at any value between about 3 and 25 p.p.m. as the tunnel incorporates a deeply buried return limb to redissolve the air which comes out of solution in the working section. This content tended to rise slowly during ventilation experiments.

3. Natural cavity pressure measurements

Difficulties similar to those experienced by Gadd & Grant (1965) in their measurements of pressure within natural, unventilated cavities behind disks, occurred in the present experiments. The technique finally used involved clearing

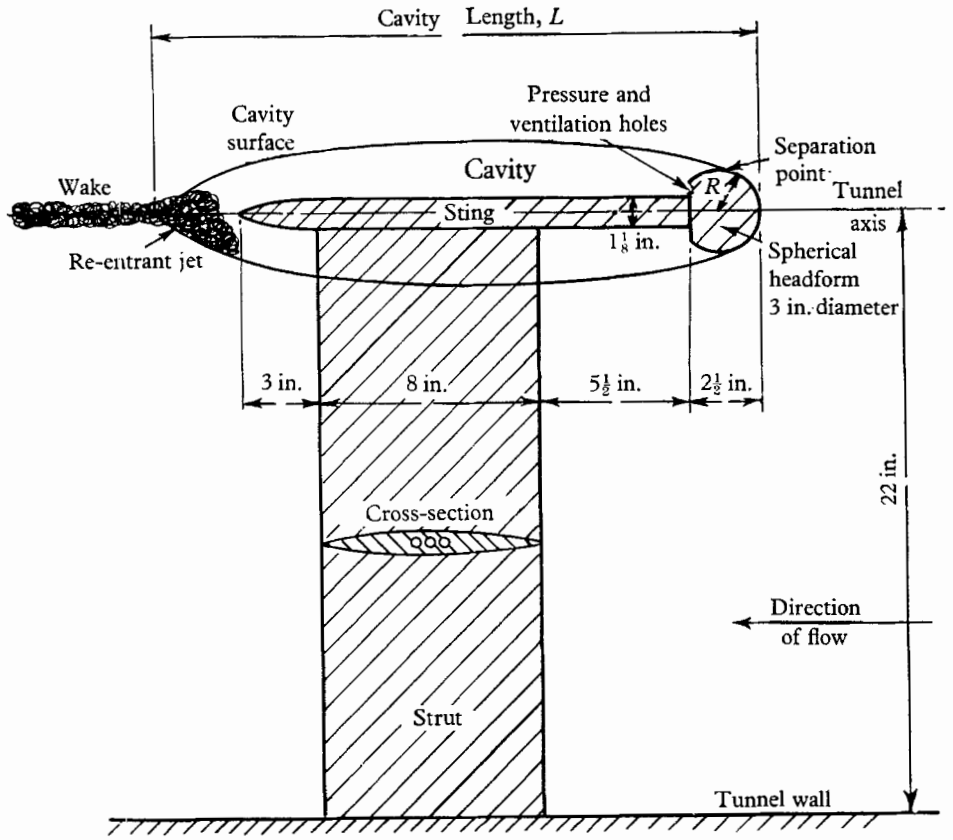

FIGURE 1. Representation of spherical headform with cavity and support system.

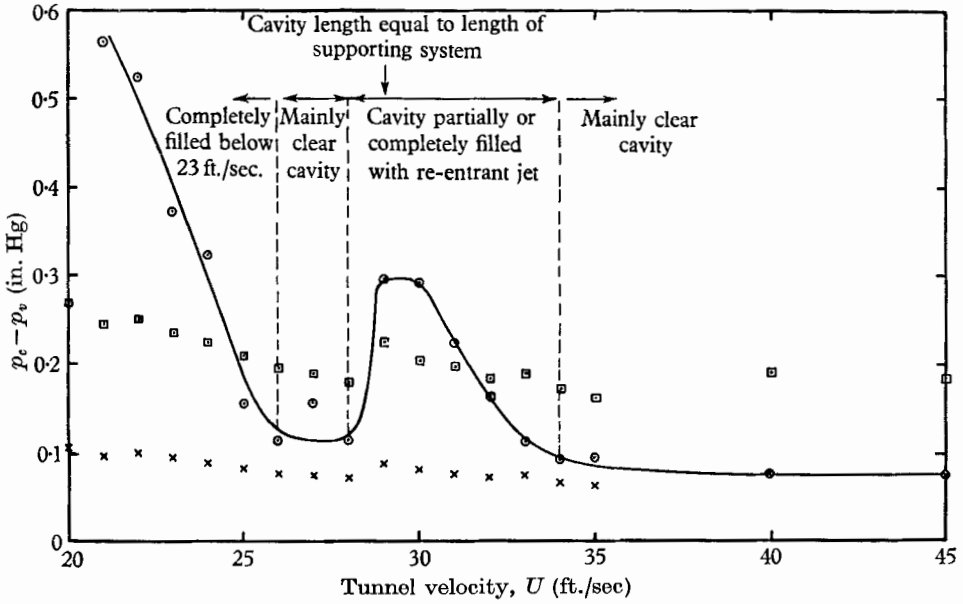

FIGURE 2. Variation of $(p_c - p_v)$ with U, air content 9·0 p.p.m. ⊙, experimental results; ⊡, turbulent boundary-layer theory; ×, adjusted theoretical points.

the pressure line to the manometer by a burst of air prior to each reading. If the tube to the manometer was opened as soon as possible after closure of the air clearing line, the pressure would then asymptote fairly quickly to a definite value. For cavities relatively empty of the turbulent fluid from the re-entrant jet, the pressure reading gave repeated values within $\pm$ 0·01 in. mercury. But when the cavity was more than about half filled by that fluid, differences as great as $\pm$ 0·05 in. Hg were likely. Further, in this latter case, the measurements may have been affected by drops of water entering the pressure line and creating a surface tension pressure.

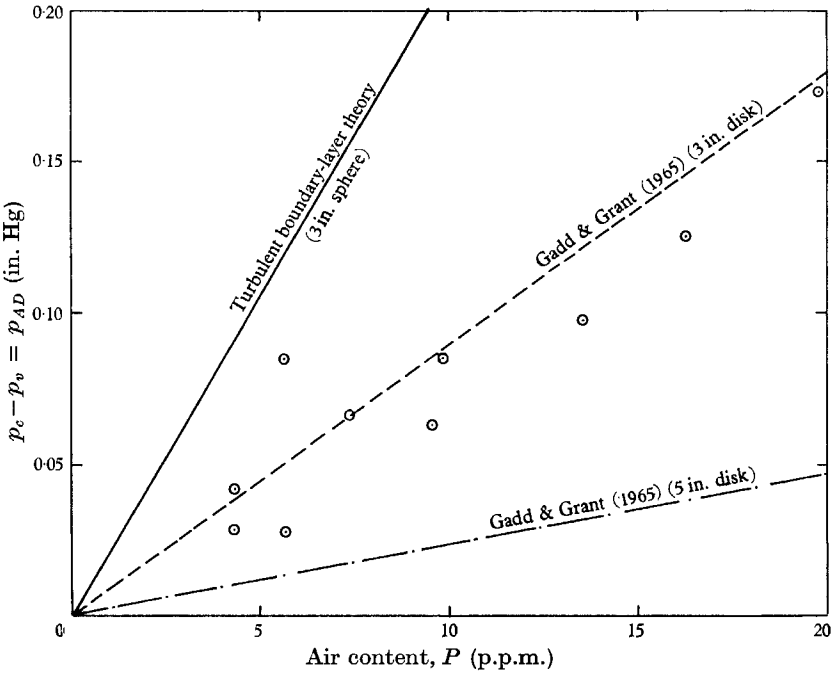

FIGURE 3. Variation of p_{AD} with P at U = 40 ft./sec, L = 3·29 ft., σ = 0·111.

At each of a number of different air contents, measurements were made for a range of speeds, the tunnel pressure (p_u) taking the lowest possible value in each case (2·2 $\rightarrow$ 3·0 in. Hg). In figure 2 ($p_c - p_v$) is plotted against U for 9·0 p.p.m. air content, the regimes of internal cavity condition being indicated. The peculiar shape of the curve was due to the physical geometry of the support system. At speeds below 28 ft./sec the cavity closed onto the supporting sting and strut, presumably muting the cavity filling effect of the re-entrant jet. Thus the cavity clears prematurely at between 26 and 28 ft./sec, only to fill again when closing downstream of the end of the sting. Finally the cavity clears at about 34 ft./sec. This coincidental effect is useful in that it would seem to indicate that there is little variation with speed of the pressure within clear cavities. Marked increase in pressure would seem to occur if the cavity is partially or completely filled, though in that case the measurements are less accurate. These results are in line with those of Gadd & Grant (1965).

Above 37 ft./sec there was little or no measurable effect of speed and the pressure measurements at 40 ft./sec ($\sigma \approx 0{\cdot}111$) are plotted against air content in figure 3. Also shown are Gadd & Grant's results for 3 and 5 in. diameter disks. Clearly there is a roughly linear relation between P and p_{AD}. The theoretical line is a result of the calculations in § 6.

4. Cavity appearance

Surface appearance of natural and ventilated cavities

Figure 4, plate 1, is a typical microflash photograph (exposure $\sim 20\,\mu$sec) taken during one of the experiments. All the cavities thus photographed whether natural or ventilated showed a clear region of surface just downstream of separation followed by a spatially growing wave pattern which breaks up to form a generally rough surface. A study of the wave patterns, which appeared to be the result of laminar boundary-layer oscillations prior to transition, was undertaken and will shortly be reported on as part of a separate investigation. In this context, their presence confirms that the boundary layer on the wetted surface is laminar for even the highest tunnel velocity (45 ft./sec). This corresponds to a Reynolds number of $9{\cdot}3 \times 10^5$ based on sphere diameter and, although well above the critical for the non-cavity flow, there is the difference that the pressure gradient is favourable over virtually all of the wetted surface in the cavitating case. For the range of speeds from 15 to 45 ft./sec transition occurred shortly after separation, the distance interval being less than $\frac{1}{2}$ in. and decreasing slightly with speed.

The 'turbulent cavity surface' of figure 4 can be compared, for example, with the clearly 'laminar cavity surface' at the forward end of the cavity behind the 5 in. disk of Gadd & Grant (1965).

Ventilated cavities

All the cases dealt with in the ventilation experiments of the next section were essentially 'steady' cavities; that is to say they were not of the 'pulsating' type described by Song (1961), the maximum operational ventilation rate being below that presumably required for pulsation in the present circumstances. The entrainment mechanism investigated by Song (1961) and Woods (1966) is thus unlikely to be relevant.

Two distinct forms of cavity closure were observed and each exhibited a different entrainment rate pattern. At lower tunnel velocities, buoyancy caused the cavity to be markedly inclined to the horizontal and to have a closure formation of the twin vortex tube type observed and investigated by Cox & Clayden (1956). However, above a critical Froude number based on cavity length (see next section) this inclination virtually disappeared and the closure was of the more regular re-entrant jet type. The experimental investigation was concentrated in the higher speed region since the buoyancy effect is uncommon, has not been reported in natural cavities and is dependent on flow orientation which the latter type of closure is not.

5. Experiments on rates of entrainment

Consider, now, what occurs when an additional supply of air to the cavity is provided by means of the ventilation facility.

M_{ID} and M_{IE} will denote the mass rates of supply of air to the cavity by diffusion and by ventilation and it is convenient to separate the partial pressures of air, p_{AD} and p_{AE} respectively, which these two supplies establish in the cavity.

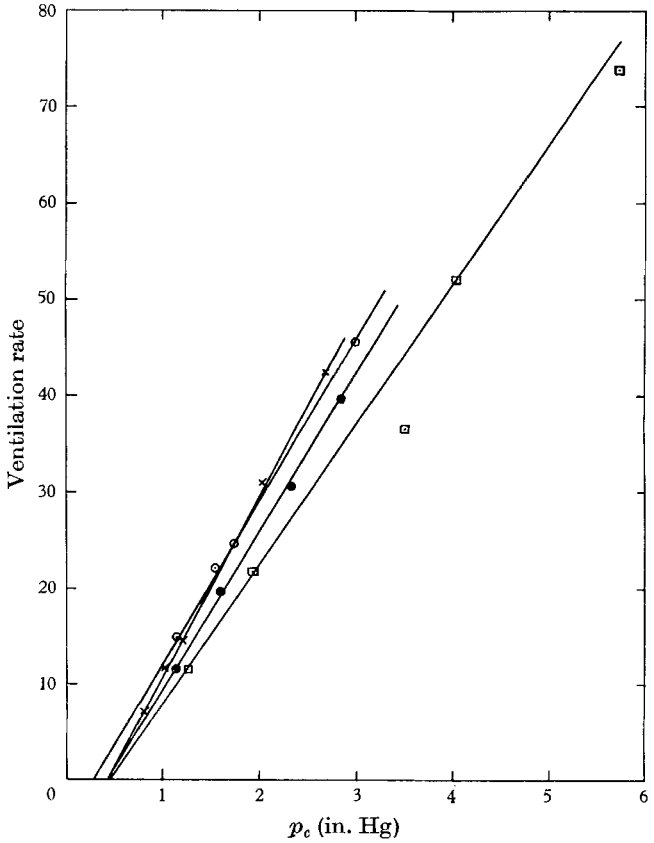

FIGURE 5. Variation of cavity pressure with ventilation rate measured as ft.^{3}/hour at N.T.P. (therefore a measure of mass rate of ventilation) for a tunnel speed, U, of 30 ft./sec. Indirect measurement: ×, L = 20 in., σ = 0·148; ⊙, L = 30 in., σ = 0·121; ⊡, L = 45 in., σ = 0·108. Direct measurement: ●, L = 30 in., σ = 0·121.

Then, in equilibrium, the total volume rate of entrainment of gas and vapour away from the cavity will be given through the perfect gas law as

$$V \propto \frac{M_{ID}}{p_{AD}} = \frac{M_{IE}}{p_{AE}}.$$

Through steam tables, V is also directly related to M_V/p_V. Thus V may be investigated by a study of one of the participant mass flows and the flow rate of ventilation is easily measured. Hence a series of experiments was carried out in which the cavity was ventilated with known mass flow rates, M_{IE}. At a particular

tunnel velocity, U, it was anticipated that the entrainment rate would depend on the size of the cavity, conveniently described by its length, L, or equivalently by the cavitation number σ, because of the one-to-one relation between L and σ for a particular headform, referred to in § 3.

For each of ten tunnel velocities between 15 and 45 ft./sec a series of conditions was set up for each of three sizes of cavity; 20, 30 and 40 in. long corresponding to $\sigma = 0{\cdot}148$, $0{\cdot}121$ and $0{\cdot}108$ (Brennen 1968). The cavity pressure, p_c, could be

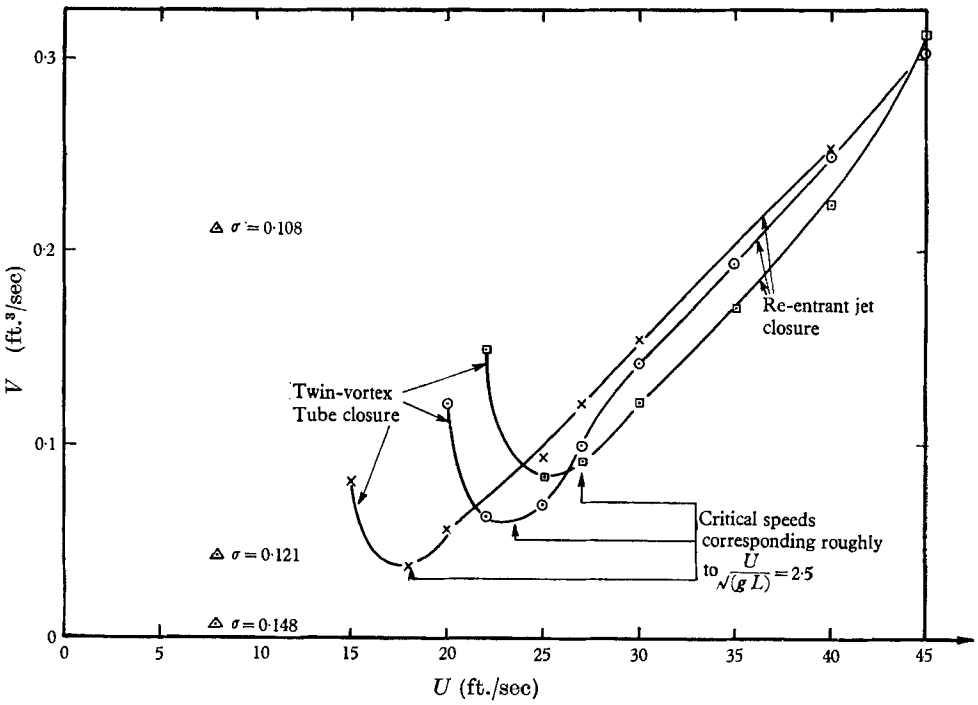

FIGURE 6. Variation of volume entrainment rate, V, with tunnel velocity and cavity size. ×, $L = 20$ in., $\sigma = 0{\cdot}148$; ⊙, $L = 30$ in., $\sigma = 0{\cdot}121$; ⊡, $L = 45$ in., $\sigma = 0{\cdot}108$; △, Cox & Clayden (1956) 1 in. diameter disk.

either measured directly or calculated using $p_u - p_c = \frac{1}{2}\rho U^2/\sigma$, knowing σ, U and p_u. Direct measurement, although necessary for confirmation of results, involved the difficulties of § 3. In addition the burst of air used to clear the pressure line temporarily upset the air input/entrainment balance. The indirect method therefore gave the more consistent and repeatable results especially at higher ventilation rates where $p_u - p_c$ is small compared with both p_u and p_c.

A typical set of results, for the case $U = 30$ ft./sec, is shown in figure 5. The vertical axis is equivalent to the mass ventilation rate, M_{IE}, being volume rate measured at constant, namely atmospheric, pressure. For each cavitation number (or cavity length) the points lay close to a straight line, the scatter tending to increase with U and L. Most of the results shown use computed values of p_c though, for comparison, a set of direct measurements (for $\sigma = 0{\cdot}121$) is given. The latter line has the same slope as its counterpart but with a slight shift of origin, probably for one of the reasons given below.

The linear nature of the results led to the conclusion that the volume rate of entrainment, $V(\propto M_{IE}/p_{AE})$ was dependent only on cavity size and tunnel velocity, the intercept on the p_c-axis being the value of $p_V + p_{AD}$ since $p_c = p_{AE} + p_V + p_{AD}$.

For all speeds the intercept was within the range between 0·15 and 0·7 in. Hg. Although some of this is experimental scatter two other reasons could account for its not being unique. The mass diffusion flow rate of air, M_{ID}, and therefore p_{AD} will depend on the *total* of the partial air pressures, $p_{AE} + p_{AD}$. This effect was eliminated as far as possible by frequent de-aeration of the tunnel in an attempt to keep p_{AD} negligible. Nevertheless, since air is constantly being introduced the air content tended to creep up during each experiment. On the other hand some of the intercepts (particularly at higher U and L) were less than the vapour pressure, p_v, at the measured operational temperature of the water. This may be due to the rapid adiabatic expansion of the air out of the ventilation system causing a significant drop in the cavity temperature.

The slopes of the lines in figure 5 and similar graphs for other speeds are converted to volume rate of entrainment and plotted in figure 6. At the higher speeds for which closure is of the re-entrant jet type the volume rate of entrainment increases sensibly with speed, U, and varies little with cavity length. Decreasing below a critical speed (corresponding roughly to $2{\cdot}5\sqrt{(gL)}$) closure changes to the twin vortex type and entrainment shows a very sharp increase, the variation with cavity length being reversed. Cox & Clayden (1956) were unfortunately restricted to a single tunnel speed of 8 ft./sec, all their cavities having the twin vortex type of closure. Although the dimensions of their flows clearly differ from those used here, the 3 in. sphere shows the same sharp increase in V with decreasing σ at about 18 ft./sec as does their 1 in. diameter disk at 8 ft./sec.

6. Theoretical estimate of the rate of diffusion of air into a natural cavity

The results of the last section indicate a possible theoretical approach by means of which the partial pressure of air, p_{AD}, in natural cavities might be predicted giving theoretical lines in figures 2 and 3. For a given U and σ, the mass flow of air out of the cavity is proportional to p_{AD}, the factor being given experimentally through figure 6. Intuitively it might be expected that the mass rate of diffusion of air into the cavity would be proportional to the air content, P, of the water. Equating inflow and outflow would yield an equation relating p_{AD} directly to P as in figure 3. Two approaches are made below to the problem of finding a theoretical estimate of the rate of diffusion of air into the cavity. But first a comment must be made on the concentration level of air in water. An upstream air content of P p.p.m. is equivalent to a concentration of $6{\cdot}24 \times 10^{-5} \times P$ lb. air/ft.^{3} water. Saturation occurs at $5{\cdot}52 \times 10^{-5} \times p_A$ lb. air/ft.^{3} water when the air pressure is p_A (in Hg) and the temperature 59 °F. Thus the water in the working section is invariably supersaturated with air above an air content of 3 p.p.m. In both diffusion approaches sufficient air is assumed to have been released to the

cavity so that the concentration at some point on the cavity surface is that of saturation at the partial pressure of air in the cavity, p_{AD}. Then the concentration difference between this point and the remote fluid, Δc, is given by

$$\Delta c = [6{\cdot}24P - 5{\cdot}52p_{AD}] \times 10^{-5} \text{ lb. air/ft.}^3 \text{ water}, \tag{1}$$

where P is in p.p.m. and p_{AD} is in Hg.

The approach of diffusion in a potential flow

Parkin & Kermeen (1963), among others, have solved the diffusion equation within a potential fluid flow to determine the flux of air into and thus the rate of growth of the minute bubbles associated with cavitation inception. A similar approach could be made with the much larger fully developed cavity. The latter can be fitted fairly simply to the mathematical model of Parkin & Kermeen as shown in figure 7*a*. A general concentration of mass of air per unit volume of water is denoted by c (lb. air/ft.^{3} water) and the theoretical potential flow velocity of the cavity surface by U_c where $U_c = U\sqrt{(1+\sigma)}$. Although the experimental cavity flow is axisymmetric the diffusion layer thickness will clearly be sufficiently small compared with the average cavity radius for a planar flow of breadth $2\pi r_a$ to give a reasonably accurate model, r_a being an average cavity radius. Then the result of Parkin & Kermeen yields the following estimate of total mass flow of air into the cavity

$$M_{ID} = 4r_a[D(L-x_s)\pi U\sqrt{(1+\sigma)}]^{\frac{1}{2}} \times \Delta c, \tag{2}$$

where Δc is given by (1) (the whole of the cavity surface being assumed to have the same concentration) and D is the diffusion coefficient whose value is quoted by those authors as 2×10^{-5} cm^2/sec.

Taking the conditions of figure 3 as an example ($U = 40$ ft./sec, $L - x_s = 3{\cdot}17$ ft, $\sigma = 0{\cdot}111$) and using, as a rough estimate, the radius of the sphere as the average cavity radius, r_a, (2) yields

$$M_{ID} = 0{\cdot}0011 \times 10^{-4}[P - 0{\cdot}885p_{AD}] \text{ lb./sec}. \tag{3}$$

Turbulent boundary-layer approach

Although the above mathematical model would be valid in the near potential flow outside the observed turbulent boundary layer on the cavity surface, it will be demonstrated that, in fact, it is this layer which plays the predominant role in the diffusion process. Making use of a consequence of Prandtl's mixing length theory it is assumed that the mechanisms for transfer of momentum and dissolved air within the turbulent boundary layer are identical. The order of accuracy expected makes any refinement on the basis, say, of G. I. Taylor's vorticity transfer theory unnecessary. The mathematical model of the flow is shown in figure 7(*b*). Then, although the air concentration profile is initially different from the velocity distribution at separation (uniform concentration as opposed to a near Blasius velocity distribution) it is assumed that they take up a geometrically similar shape before the end of the cavity. Denoting a velocity and a concentration within the layer by u and c respectively and the corresponding deficits by $u_1 = U_c - u$ and $c_1 = c_\infty - c$ (c_∞ being the concentration of the remote fluid) then

$$u_1/(u_1)_{y=0} = c_1/(c_1)_{y=0} = f(y). \tag{4}$$

The difference between the flux of air within the boundary layer at a particular x position and the flux of air had none been released to the cavity, is termed the 'lost air flux' and is given, per unit depth of field, by

$$\Delta M = \int_0^\infty c_1(U_0 - u_1)\, dy.$$

This, in fact, is the air flowing down the cavity itself past that x position. Thus performing the integral at $x = L$ yields the total flow of air into and out of the cavity, i.e.

$$M_{ID} = 2\pi r_a(c_\infty - c_{y=0,\,x=L})\, U_c \int_0^\infty f(y)\left[1 - \frac{(u_1)_{y=0,\,x=L} f(y)}{U_c}\right] dy. \tag{5}$$

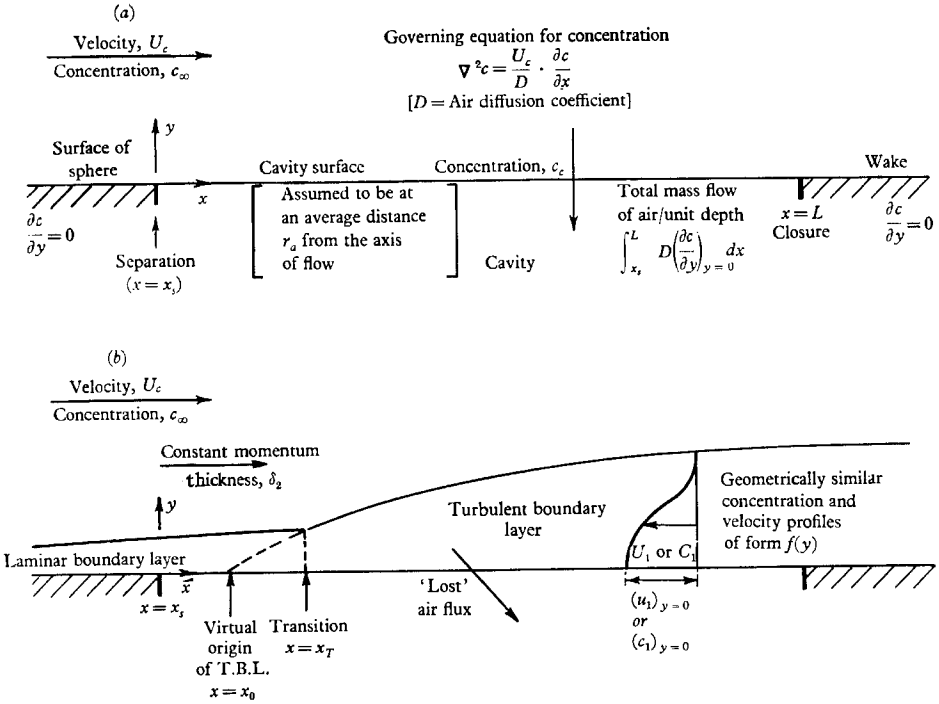

FIGURE 7. Models for diffusion of air into cavity. (*a*) Potential flow diffusion model. (*b*) Turbulent boundary-layer model.

Now in the straight cavity surface approximation the turbulent boundary layer has the same boundary conditions as half the wake flow behind a flat plate parallel to the stream. The momentum thickness, δ_2, is constant along the free streamline. For all the cases treated the value of δ_2/L is so small that, following Townsend (1956), $f(y)$ can be assumed to be the Gaussian function

$$f(y) = \exp\left[-\left(\frac{\pi}{2}\right)^{\frac{1}{2}} \frac{R_T}{4\delta_2} \frac{y^2}{x - x_0}\right], \tag{6}$$

where x_0 is the virtual origin of the turbulent boundary layer and R_T is a constant equal to 12·5. Similarly it is easily shown that for the relevant values of (δ_2/L) the $[f(y)]^2$ term in (5) makes a negligible contribution to the result.

The value of δ_2 is a function of the particular headform and the wetted surface velocity distribution. Using the pressure distributions given by Brennen (1968) for the wetted surface of a cavitating sphere and the approximate integral method of Rott & Crabtree (1952) δ_2 was found to be given by $I\sqrt{(R\nu/U)}$ (R and ν being the radius of the sphere and the kinematic viscosity) where I was estimated as 0·3, varying negligibly with cavitation number within the range $0 < \sigma < 0{\cdot}4$.

Since transition occurred so close to separation (§ 4) it can be easily shown that the assumption of the separation point as the virtual origin ($x_0 = x_s \approx 1\frac{1}{2}$ in.) of the turbulent boundary layer involves little error.

Finally (5) yields

$$M_{ID} = 2{\cdot}82(c_\infty - c_{y=0,\,x=L})\, U^{\frac{3}{4}}(L-x_s)^{\frac{1}{2}}(R\nu)^{\frac{1}{4}}I^{\frac{1}{2}}(1+\sigma)^{\frac{1}{2}}r_a. \tag{7}$$

As a first approximation it is assumed that sufficient mixing has taken place along the length of the free surface, $(L-x_s)$, for the concentration on the cavity surface, $y = 0$, to have been lowered to the saturation level at the cavity air pressure, p_{AD}. Then $(c_\infty - c_{y=0,\,x=L})$ will be given by the expression for Δc in (1). It is to be noted that this would yield the maximum air flux, M_{ID}, possible.

In the present case putting $I = 0{\cdot}3$, $\nu = 1{\cdot}21 \times 10^{-5}$ and as before, $r_a = 1\frac{1}{2}$ in., (7) becomes

$$M_{ID} = 0{\cdot}427 \times 10^{-6}[P - 0{\cdot}885p_{AD}]\, U^{\frac{3}{4}}(L-x_s)^{\frac{1}{2}}(1+\sigma)^{\frac{1}{2}}, \tag{8}$$

where P is in p.p.m. and p_{AD} in in. mercury. For the conditions of figure 3 this becomes

$$M_{ID} = 0{\cdot}127 \times 10^{-4}[P - 0{\cdot}885p_{AD}]\,\text{lb./sec}. \tag{9}$$

This influx of air far exceeds that predicted by potential diffusion theory alone in (2) and (3).

7. Dynamic air balance for natural cavities

The theory outlined in the last section can be tested by matching the mass diffusion rate it predicts with what must in equilibrium be an equal entrainment rate. The volume entrainment rate, V, has been found experimentally (figure 6). For example, under the conditions of figure 3, $V = 0{\cdot}23\,\text{ft.}^3/\text{sec}$ and the mass influx of dissolved air must therefore be $0{\cdot}587 \times 10^{-3} \times p_{AD}$ lb./sec. Equating this with (9) yields

$$\underset{\text{(in. Hg.)}}{p_{AD}} = 0{\cdot}0212\underset{\text{(p.p.m.)}}{P}.$$

This theoretical line is shown in figure 3. Through equation (3), potential diffusion alone would make $p_{AD} = 0{\cdot}000187P$.

Although the simplification involved in the theory would in any case preclude any great accuracy, it would nevertheless appear that the turbulent boundary-layer approach is basically correct, in contrast with that which considers potential diffusion alone. The air influx, M_{ID}, appears to have been overestimated which would lead one to conclude that the saturation level has not, in fact, quite been reached on the cavity surface. The error is therefore on the right side. Other unknown factors include the influence of curvature on the development of the turbulent boundary layer.

Equation (8) has also been used in conjunction with figure 6 to predict values corresponding to each of the experimental points in figure 2 (the irregularities are

due to local differences in p_u, L and σ). Also shown is the same curve scaled down by assuming a uniform percentage saturation level attainment which would make the values at 40 ft./sec coincide. The values given for the lower speeds at which the cavities are shorter than 20 in. are based on extrapolated values of entrainment rate from figure 6. This extrapolation is probably inaccurate when the cavity fills with re-entrant fluid. If this fluid hinders entrainment, it would account for the considerably increased pressure under those conditions.

Reverting to figure 3, the results of Gadd & Grant (1965) provide a qualitative comparison with theory. Their 3 in. disk was supported by wires piercing the surface and causing transition just downstream of separation. The p_{AD}/P curve is then of the same order as that for the 3 in. sphere. On the other hand their photographs show that in the case of the 5 in. disk the surface boundary layer remains laminar for the greater proportion of the length of the cavity. This would account for the much reduced air influx and cavity pressure per unit air content.

8. A note on the heat balance for natural cavities

In a natural cavity heat is taken from the stream to provide a continuous creation of water vapour at the cavity surface. Making the same assumptions about the transfer of heat as for the transfer of dissolved air, the heat flux to the cavity is given by the expression, (7), but with the concentrations, c, of air replaced by the corresponding heat contents. Denoting the upstream and cavity temperatures by T_u and T_c (°F) and the latent heat of vaporization at T_c by l (B.Th.U./lb.), the flux of vapour through the cavity is

$$M_V = \frac{176(T_u - T_c)}{l} [U^{\frac{3}{4}}(L - x_s)^{\frac{1}{2}} (R\nu)^{\frac{1}{4}} I^{\frac{1}{2}}(1+\sigma)^{\frac{1}{2}} r_a] \tag{10}$$

in lb./sec. Take again the example of figure 3 conditions; from figure 6 $V = 0{\cdot}23$ ft.^{3}/sec and, at the operating temperature of 59 °F, steam tables yield $M_V = 0{\cdot}184 \times 10^{-3}$ lb./sec. Equating this with (10), the temperature difference $(T_u - T_c)$ computes as 0·025 °F. It is easily seen that at any tunnel speed within the operating range the difference, $(T_u - T_c)$, is minute.

As in the parallel air diffusion problem a purely potential flow approach would predict much smaller values for $M_V/(T_u - T_c)$ than (10) and therefore temperature differences of the order of 3 or 4 °F. Eisenberg & Pond (1948) performed temperature measurements within a cavity flow similar to that employed in the present paper and could detect no variation above a resolution of 0·04 °F. This seems to confirm that the potential flow approach underestimates the influx to the cavity by at least two orders of magnitude.

9. Concluding remarks

Although the cavities studied in this investigation were of a relatively simple type, nevertheless some insight has been gained into the mechanisms of the dissolved air and heat equilibriums of any cavity flow. The turbulent boundary layer on the cavity surface clearly plays a major role in the inward diffusion processes.

Dissolved air and heat balances have been set up using theoretically derived rates of diffusion out of this layer into the cavity and experimentally obtained entrainment rates away from the cavity. The dissolved air equilibrium predicts the experimentally verified linear relation between air content of the water and partial pressure of air in natural 'clear' cavities. The factor of proportionality, p_{AD}/P, is overestimated since the theory yields a maximum inward rate of diffusion of air. When the cavity is partially or completely filled with re-entrant fluid it may be that the hindering of entrainment this produces accounts for the considerable increase in cavity pressure. The heat balance indicates that the temperature differences within a natural cavity flow are likely to be virtually undetectable.

The other interesting conclusion which can be made also concerns ventilated cavities. The results of § 5 indicate that the volume rate of entrainment of all gas and vapour is dependent only on water speed and cavity size for steady cavities behind a particular headform. This result seems reasonable and may be true for all steady cavities.

This work is part of the research programme of the Ship Division of the National Physical Laboratory. The author wishes to thank Mr S. Grant for assistance in carrying out the experimental investigation and Dr G. E. Gadd for valuable discussions on the subject.

REFERENCES

BRENNEN, C. 1968 A numerical solution of axisymmetric cavity flows. Parts I and II. *N.P.L. Ship Division Report*, no. 114.

COX, R. N. & CLAYDEN, W. A. 1956 Air entrainment at the rear of a steady cavity. *Symp. on Cavitation in Hydrodynamics*. N.P.L. Sept. 1956. London: H.M.S.O.

EISENBERG, P. & POND, H. L. 1948 Water tunnel investigations of steady state cavities. *David Taylor Model Basin Report*, no. 668.

GADD, G. E. & GRANT, S. 1965 Some experiments on cavities behind disks. *J. Fluid Mech.* **23**, 4.

PARKIN, B. R. & KERMEEN, R. W. 1963 The roles of convective air diffusion and liquid tensile stresses during cavitation inception. *Proc. Iahr Symp. on Cavitation and Hydraulic Machinery*, Sendai, Japan, 1963.

ROTT, N. & CRABTREE, L. F. 1952 Simplified laminar boundary layer calculations for bodies of revolution and for yawed wings. *J. Aero. Sci.* **19**, 553–65.

SILVERLEAF, A. 1960 Basic design of the N.P.L. no. 2 water tunnel. *N.P.L. Ship Division Report*, no. 15.

SONG, C. S. 1961 Pulsation of ventilated cavities. *Univ. of Minnesota, St Anthony Falls Hydraulic Lab. Tech. Paper*, no. 32, series B.

TOWNSEND, A. A. 1956 *The Structure of Turbulent Shear Flow*. Cambridge University Press.

WOODS, L. C. 1966 On the instability of ventilated cavities. *J. Fluid Mech.* **26**, 437–57.

FIGURE 4. Microflash photograph of ventilated cavity at $U = 30$ ft./sec, $\sigma = 0{\cdot}127$.